LES of Turbulence Features of Turbulent Forced Convection of Pseudoplastic and Dilatant Fluids, chapitre 11

Meryem Ould-Rouiss, Mohamed Abdi, Lalia Abir Bouhenni, Fatima Zohra Nedjda Bouhenni, Nour Elhouda Beladjine, Manel Ait Yahia

11 LES of Turbulence Features of Turbulent Forced Convection of Pseudoplastic and Dilatant Fluids

Mohamed Abdi, Meryem Ould-rouiss, Lalia Abir Bouhenni, Fatima Zohra Bouhenni, Nour Elhouda Beladjine, and Manel Ait Yahia

11.1 INTRODUCTION

Turbulent flow in pipes has been a famous benchmark case for testing and evaluating theories and turbulence models during the past century. Turbulence is among the most complicated issues in fluid dynamics. During the previous few decades, researchers in mechanics and engineering have shown great interest in Newtonian fluids of turbulent flow in axial pipes.

This flow is significant in the industrial domains. It involves several technical applications, including heat exchange, flow in nuclear reactors, and turbomachinery.

As part of their research, mechanics and engineering are interested in turbulent flows of non-Newtonian fluids. Various engineering and industrial applications often use this field. There are several applications where non-Newtonian fluids are used, including drilling hydraulics, wastewater transportation, slurries, pastes, suspensions of solids in liquids, emulsions, mineral oil processing, arterial blood flow, and other applications involving relatively high heat transfer rates. Fluids may also show Newtonian and non-Newtonian behavior, depending on their shear rate and their characteristic relationship to Newtonian behavior.

In these engineering applications, the turbulent flow of non-Newtonian fluids in a straight pipe is of great practical interest, where numerous studies have been performed in the last decades to better understand the behavior of this kind of fluids. A review of the literature suggests that the hydrodynamic field of fully evolved turbulent Non-Newtonian fluid flow has attracted a lot of interest in recent decades, either experimentally [1–5] or numerically by [6–17].

Abdi et al. [18] conducted LES with an extended Smagorinsky model to simulate fully developed turbulent forced convection of thermally impartial pseudoplastic fluids with a flow behavior index of 0.75 through an axially heated rotating pipe. With a rotation rate ranging from 0 to 3, the simulation Re and Pr numbers of the working fluid were assumed to be 4,000 and 1, respectively. It is observed that as the pipe wall rotates, it is seen that the temperature along its radius noticeably decreases as the rotation rate increases. This is due to a drop in apparent fluid viscosity in the pipe's core region, which causes a centrifugal force that causes the mean axial velocity profile to increase noticeably.

Convective heat transfer flows are often encountered in mechanical and chemical engineering fields, such as fluid machinery, mixing and chemical reaction enhancement in the combustion chamber, etc. Recently, several studies have been carried out on the heat transfer process of nanofluids in magnetohydrodynamic (MHD) presence. Many researchers have conducted extensive research among them to gain a deeper understanding of this phenomenon [19–24].

This literature review demonstrates that previous research has primarily concentrated on the hydrodynamic field, although the interest in forced convection heat transfer in the engineering noted

DOI: 10.1201/9781003299608-11

earlier currently lacks more details on such an issue. The overall aims of the present investigation are to explore the flow behavior index influence of the power-law fluid on the main thermal turbulent statistics, especially at the wall vicinity, to describe the thermal turbulence features, in addition to shedding further light on the transfer mechanism of the turbulent energy of this kind of fluids. To this end, a fully formed turbulent forced convection of thermally independent power-law fluids through a uniform heated pipe has been numerically investigated using LES with a standard dynamic model. The flow behavior index was chosen to be 0.75 (pseudoplastic), 1 (Newtonian), and 1.2 (dilatant) at simulation Re and Pr numbers equal to Re_s = 4,000 and Pr_s = 1, respectively, where the computations are based on a finite difference scheme, second-order accurate in space and in time, and has a numerical resolution of 65^3 gridpoints in r, θ, and z directions and with domain length of $20R$. Organizing the present chapter is as follows: governing equations and numerical procedure are presented in Section 2. The effects of flow behavior index on the main thermal turbulent statistics are presented in Section 3. This research concludes with a summary and conclusion in Section 4.

11.2 GOVERNING EQUATIONS AND NUMERICAL PROCEDURE

11.2.1 Governing Equations

A numerical analysis is presented in the present study using the LES approach with a fully developed turbulent forced convection of pseudoplastic ($n = 0.75$), Newtonian ($n = 1$), and dilatant ($n = 1.2$) fluids through a uniform heated pipe (Figure 11.1), at Re_s equal to Re_s = 4,000 and Pr equal Pr_s = 1.

According to this definition, the dimensionless temperature is:

$$\Theta = \left(\left\langle T_w(z)\right\rangle - T(\theta, r, z, t)\right)/T_{ref} \tag{11.1}$$

Where T_w is the wall temperature and < > is the average in time and periodic directions.

Based on the filtered equations, we can write them as follows:

$$\frac{\partial \overline{u}_i}{\partial x_i} = 0 \tag{11.2}$$

$$\frac{\partial \overline{u}_j}{\partial t} + \frac{\partial \overline{u}_i \overline{u}_j}{\partial x_i} = -\frac{d\overline{P}}{\partial x_j} + \frac{1}{\mathrm{Re}_s}\frac{\partial}{\partial x_i}\left[\overline{\dot{\gamma}^{n-1}}\left(\frac{\partial \overline{u}_j}{\partial x_i} + \frac{\partial \overline{u}_i}{\partial x_j}\right)\right] + \frac{\partial \overline{\tau}_{ij}}{\partial x_i} \tag{11.3}$$

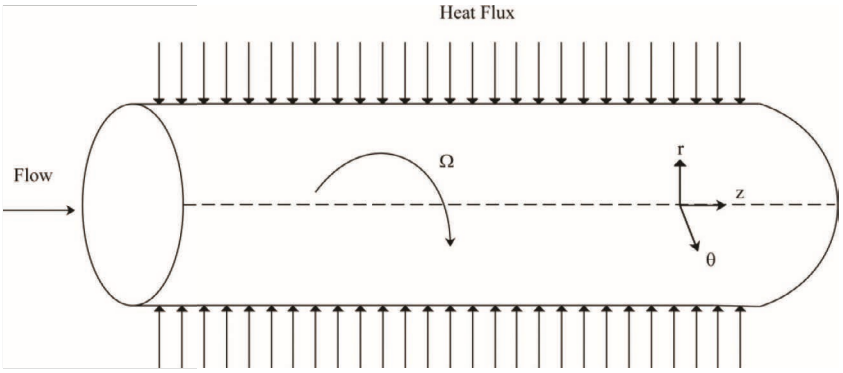

FIGURE 11.1 Physical configuration of the problem.

$$\frac{\partial \bar{\Theta}}{\partial t}+\frac{\partial}{\partial x_j}\left(\bar{u}_j\bar{\Theta}-T_{\Theta j}\right)-\bar{u}_z\frac{d}{dz}\langle T_w\rangle=\frac{1}{\mathrm{Re}_s\,\mathrm{Pr}_s}\frac{\partial^2\bar{\Theta}}{\partial x_k\partial x_k} \tag{11.4}$$

T_{ref}, Re_s, and Pr_s denote the reference temperature, simulation Reynolds number, and simulation Prandtl number, respectively, and are defined by: $T_{ref} = q_w/\rho U_{CL}C_p$, $Re_s = \rho U_{CL}^{2-n}R^n/K$, and $Pr_s = \mu/\rho\alpha U_{CL}^{1-n}R^{n-1}$, respectively.

11.2.2 Numerical Procedure

Staggered meshes with a computational length of $20R$ were used to discretize the governing equations. In order to compute the numerical integration, a finite difference method with second-order spatial and temporal accuracy was employed. A fractional-step approach is used for the time progress. Convective and diffusive terms were evaluated using third-order Runge–Kutta explicit schemes and Crank–Nicolson implicit schemes, respectively. A finite difference laboratory code was used to implement the aforementioned mathematical model. It is in agreement with the available literature data that 65^3 grid points provided a reliable forecast of turbulence statics in axial, radial, and circumferential directions; however, they also provided an excellent compromise between the required CPU time and accuracy.

For the axial and circumferential directions, periodic boundary conditions are applied, while no-slip boundary conditions are usually employed for the pipe wall. An axial and circumferential uniform grid was used; otherwise, non-uniform meshes were specified in the radial direction.

11.3 RESULTS AND DISCUSSION

The findings of fully developed turbulent forced convection of thermally independent Ostwald–de Waele fluids inside a uniformly heated axially stationary pipe are analyzed and discussed in this section. The flow behavior index was chosen to be 0.75, 1, and 1.2 at simulation Reynolds and Prandtl numbers equal to Re_s = 4,000 and Pr_s = 1, respectively. This is to demonstrate the flow behavior index's impact on the main thermal turbulence statistics.

For validation purposes, the current LES predictions were compared relatively favorably with the available results of the literature: direct numerical simulation results obtained of a Newtonian fluid ($n = 1$) at Re = 5,500 reported by Redjem et al. [25]. Figure 11.2 reasonably compares the present Newtonian radial heat flux profile with Redjem et al. [25]. As seen in Figure 11.2, the present profile is in excellent agreement with the DNS data of Redjem et al. [25] throughout the pipe radius, when there are no discernible variations in the radial coordinate.

11.3.1 Root Mean Square of Temperature Fluctuations

The effects of the flow behavior index on the temperature turbulence intensities of the pseudoplastic, Newtonian, and dilatant fluids are discussed in the present section. Figure 11.3 shows the root mean square (RMS) of the temperature fluctuations distributions of pseudoplastic ($n = 0.75$), Newtonian ($n = 1$), and dilatant ($n = 1.2$) fluids against the distance from Y^+ at Re_s = 4,000 and Pr_s = 1.

As illustrated in Figure 11.3, temperature turbulence intensities profiles are almost completely independent of the flow behavior index near the pipe wall, where these profiles are consistent with each other in the viscous sublayer ($0 \le Y^+ \le 5$). The RMS profiles deviate from each other with the wall distance from the wall towards the core region, where the flow behavior index influence becomes significant further away from the wall. As shown in Figure 11.3, there were no appreciable differences between the RMS of the pseudoplastic and Newtonian fluids along the radial coordinate. In contrast, the RMS of the dilatant fluid lies down the pseudoplastic and Newtonian fluids along the pipe radius, where this deviation is more pronounced in the buffer ($5 \le Y^+ \le 30$)

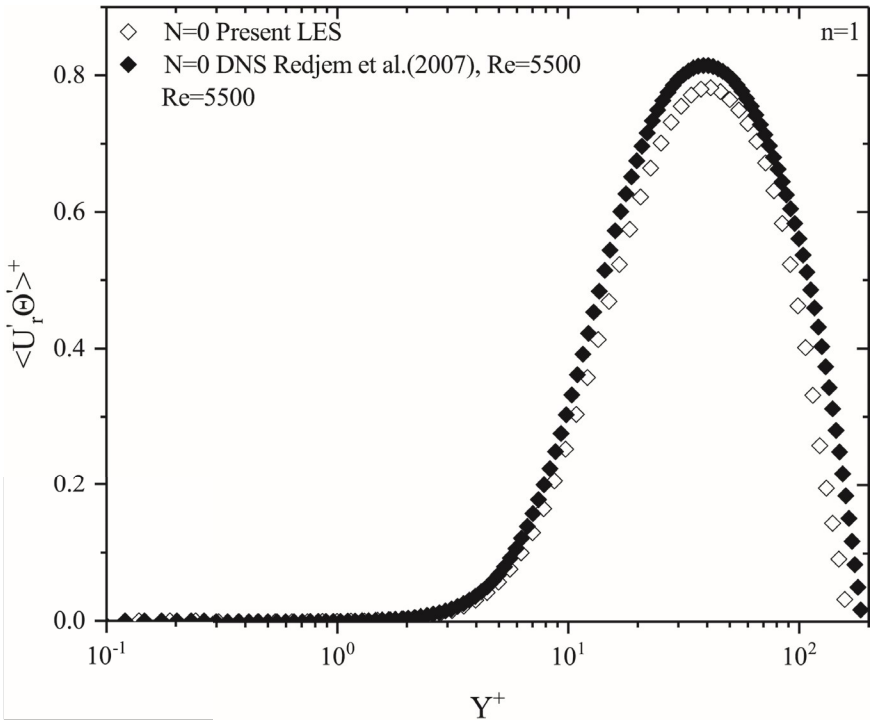

FIGURE 11.2 Validation.

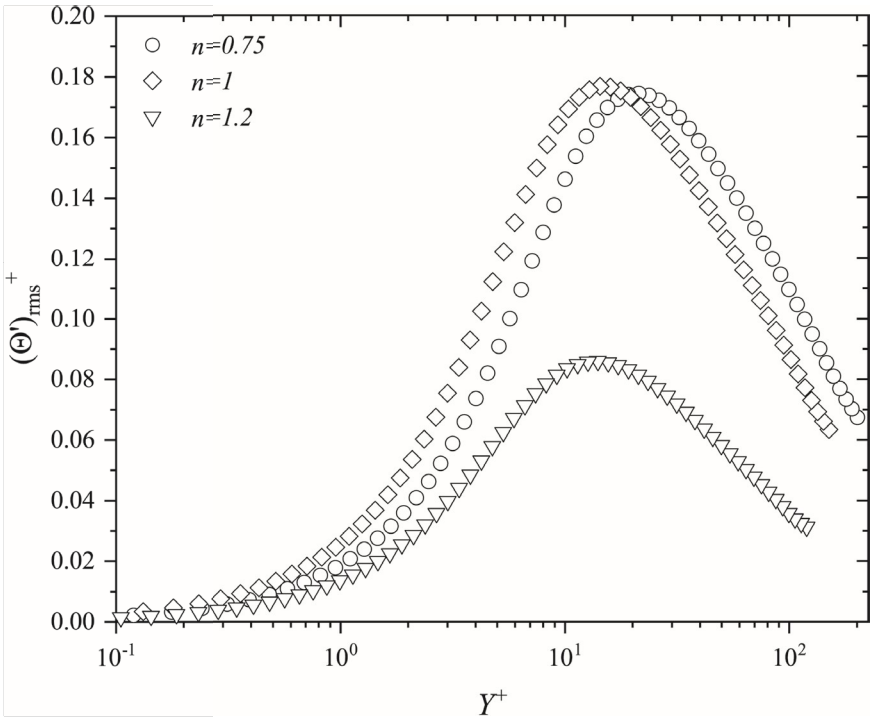

FIGURE 11.3 Temperature fluctuation RMS.

and logarithmic ($30 \leq Y^{+} \leq 200$) regions. The improved flow behavior index (n) results in a noticeable attenuation in the temperature turbulence intensities of the Ostwald–de Waele fluids along the radial coordinate.

11.3.2 The Turbulent Heat Flux of Temperature Fluctuations

The next paragraphs address the effect of the flow behavior index on the turbulent heat flux of temperature changes in power-law fluids, where the radial and axial heat flux profiles of the pseudoplastic, Newtonian, and dilatant fluids are presented respectively in Figure 11.4 and Figure 11.5. Figure 11.4 and Figure 11.5 illustrate the axial and radial heat flux profiles distributions of shear-thinning ($n = 0.75$), Newtonian ($n = 1$), and shear-thickening ($n = 1.2$) fluids against the distance from the wall in wall units Y^{+} at $Re_s = 4{,}000$ and $Pr_s = 1$.

As what appear in Figure 11.4 and Figure 11.5, the flow behavior index has little effect on the heat flux profiles near the wall, and the axial and radial heat flux profiles are nearly identical along the viscous sublayer, where these profiles are consistent totally with each other in the vicinity of the pipe wall. Interestingly, the axial and radial heat flux of the shear-thinning and Newtonian fluids are almost identical along the pipe radius, while the axial and radial heat flux of the shear-thickening fluids lie further bottom of the Newtonian fluid; this trend is more noticeable in the buffer region. It can be argued that the axial and radial heat flux along the pipe radius is significantly reduced due to the elevated flow behavior index.

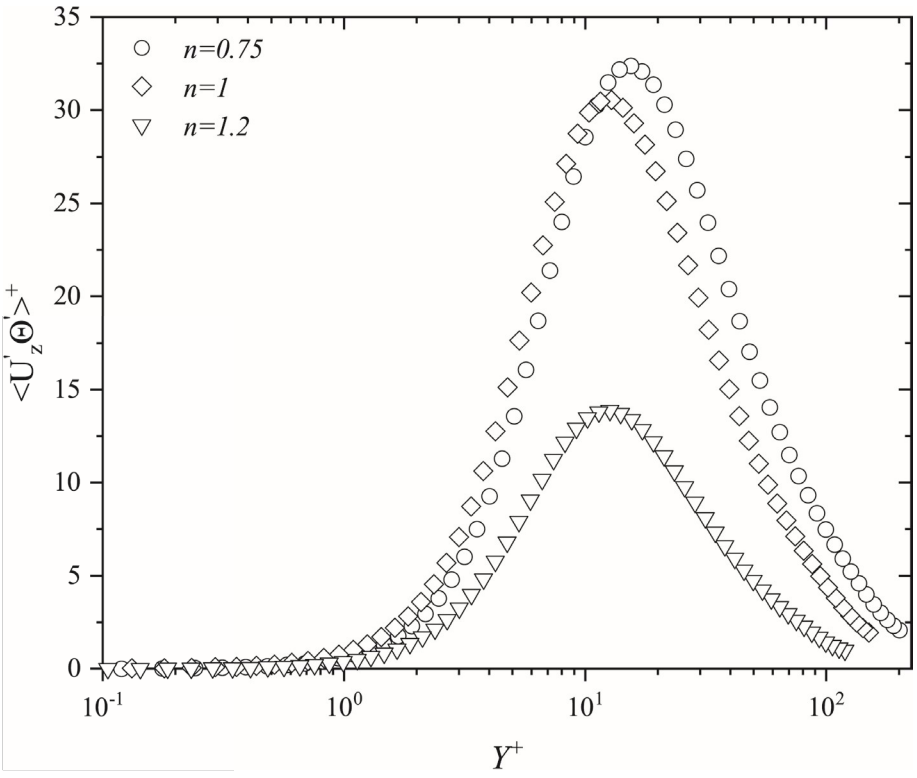

FIGURE 11.4 Heat flux axially turbulent.

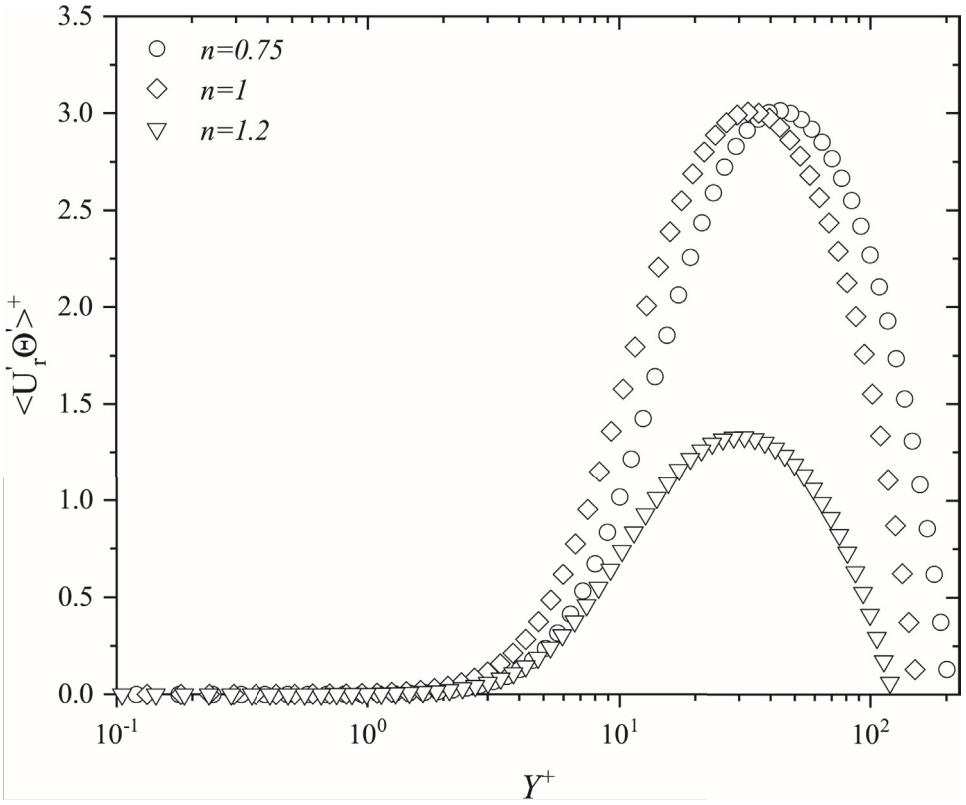

FIGURE 11.5 Radial turbulent heat flux.

11.3.3 Higher-Order Statistics

The flow behavior index and its effect on the higher-order statistics of the temperature fluctuation of the pseudoplastic, in the following paragraph, Newtonian and dilatant, fluids are analyzed and discussed. Figure 11.6 and Figure 11.7 show the skewness and flatness profiles of the temperature fluctuation of pseudoplastic ($n = 0.75$), Newtonian ($n = 1$), and shear-thickening ($n = 1.2$) fluids against the distance from Y^+ at $Re_s = 4{,}000$ and $Pr_s = 1$.

The skewness of the temperature fluctuations is essential in the vicinity of the wall compared to that in the core region; its trend decreases rapidly near the wall towards the core region with the distance from the wall, which tends to be 0 (Gaussian value) for the flow index. The flatness of the temperature fluctuations has the same trend as the skewness one; the flatness profile drops to 4 (Gaussian value) for all flow behavior indices, as shown in Figure 11.7. It can be said that the skewness and flatness of temperature fluctuations are almost independent of flow behavior index.

11.4 CONCLUSIONS

In the present research, the large-eddy simulation (LES) approach with a standard dynamic model is numerically investigated to develop turbulent forced convection of thermally independent power-law fluids through a uniform heated pipe. The flow behavior index was chosen to be 0.75 (pseudoplastic), 1 (Newtonian), and 1.2 (dilatant) at simulation Reynolds equal to $R_{es} = 4{,}000$ and Prandtl

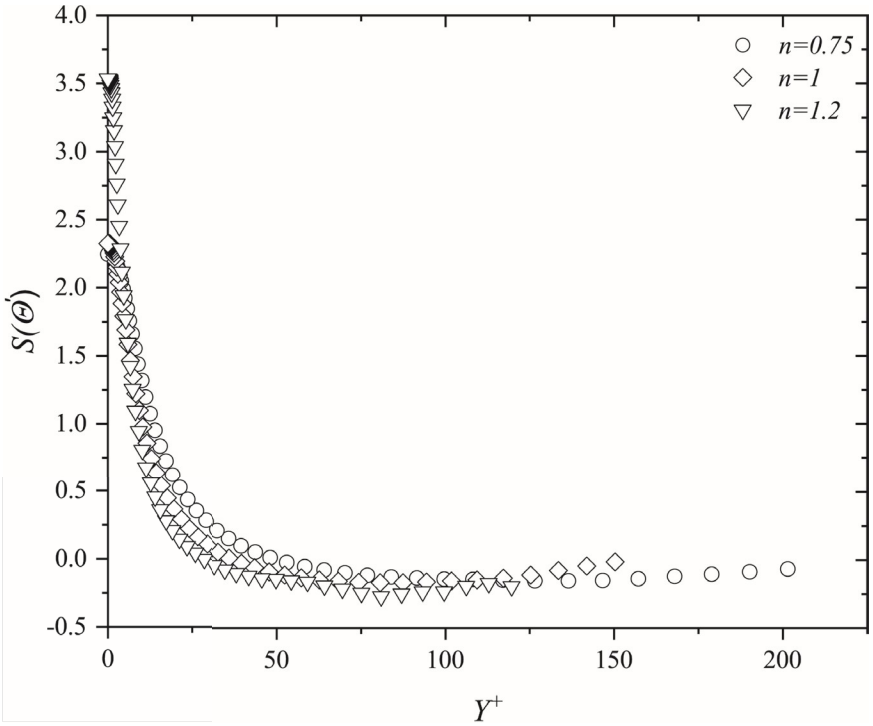

FIGURE 11.6 Skewness of temperature fluctuations.

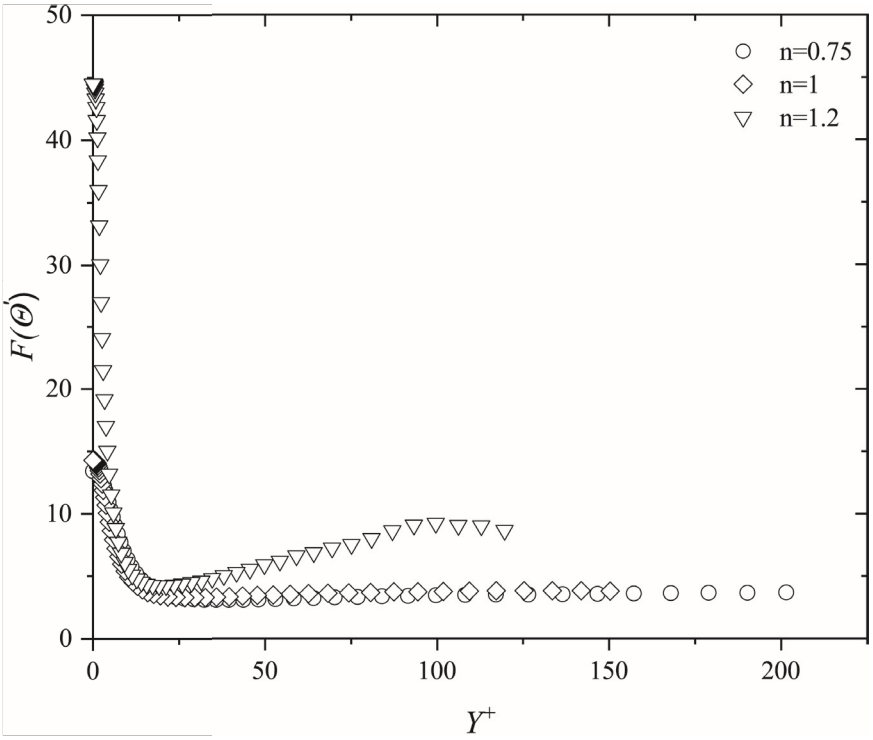

FIGURE 11.7 Flatness of temperature fluctuations.

numbers equal to $P_{rs} = 1$, where the computations are based on a finite difference scheme, second-order accurate in space and in time, and have a numerical resolution of 65^3 gridpoints in r, θ, and z directions, with computational domain length of $20R$.

The current study aimed to investigate the flow behavior index influence of the power-law fluid on the main thermal turbulent statistics to describe the thermal turbulence features of this kind of fluid. The predicted turbulent statistics agreed well with DNS data results.

The major conclusions of this research are summarized thusly:

- The increased flow behavior index produces a noticeable attenuation in the power-law fluids' temperature turbulence intensities along the radial coordinate.
- Interestingly, the axial and radial heat flux of the shear-thinning and Newtonian fluids are almost identical along the pipe radius, while the shear-thickening fluids axial and radial heat fluxes are located deeper bottom of the Newtonian fluids; this pattern is more evident in the buffer zone. It can be argued that the axial and radial heat flux along the pipe radius is significantly reduced due to the elevated flow behavior index.
- Temperature fluctuations depend almost completely on flow behavior along the radial coordinate.

Future studies will address the following subject matter:

- A fully developed turbulent flow of another non-Newtonian fluid, such as Bingham–Herschel–Bulkley and Casson fluids in pipes using LES
- The turbulent flow of Ostwald–de Waele fluid employing the direct numerical simulation (DNS)

Nomenclature

n	power-law index
Re_s	simulation Reynolds number
Pr_s	simulation Prandtl number
η	apparent viscosity
ρ	density
Y^+	distance from the wall in wall units
U^+	mean axial velocity in wall units

REFERENCES

1. Metzner, A. B., & Reed, J. C. (1955). Flow of non-newtonian fluids—correlation of the laminar, transition, and turbulent-flow regions. *AIChE Journal*, 1(4), 434–440.
2. Metzner, A. B. (1957). Non-Newtonian fluid flow. Relationships between recent pressure-drop correlations. *Industrial & Engineering Chemistry*, 49(9), 1429–1432.
3. Dodge, D. W., & Metzner, A. B. (1959). Turbulent flow of non-Newtonian systems. *AIChE Journal*, 5(2), 189–204.
4. Vidyanidhi, V., & Sithapathi, A. (1970). Non-Newtonian flow in a rotating straight pipe. *Journal of the Physical Society of Japan*, 29(1), 215–219.
5. Pinho, F. T., & Whitelaw, J. H. (1990). Flow of non-Newtonian fluids in a pipe. *Journal of Non-Newtonian Fluid Mechanics*, 34(2), 129–144.
6. Malin, M. R. (1997). Turbulent pipe flow of power-law fluids. *International Communications in Heat and Mass Transfer*, 24(7), 977–988.
7. Malin, M. R. (1997). The turbulent flow of Bingham plastic fluids in smooth circular tubes. *International Communications in Heat and Mass Transfer*, 24(6), 793–804.
8. Malin, M. R. (1998). Turbulent pipe flow of Herschel-Bulkley fluids. *International Communications in Heat and Mass Transfer*, 25(3), 321–330.

9. Rudman, M., Blackburn, H. M., Graham, L. J., & Pullum, L. (2004). Turbulent pipe flow of shear-thinning fluids. *Journal of Non-Newtonian Fluid Mechanics*, 118(1), 33–48.
10. Rudman, M., & Blackburn, H. M. (2006). Direct numerical simulation of turbulent non-Newtonian flow using a spectral element method. *Applied Mathematical Modelling*, 30(11), 1229–1248.
11. Ohta, T., & Miyashita, M. (2014). DNS and LES with an extended Smagorinsky model for wall turbulence in non-Newtonian viscous fluids. *Journal of Non-Newtonian Fluid Mechanics*, 206, 29–39.
12. Gnambode, P. S., Orlandi, P., Ould-Rouiss, M., & Nicolas, X. (2015). Large-eddy simulation of turbulent pipe flow of power-law fluids. *International Journal of Heat and Fluid Flow*, 54, 196–210.
13. Gavrilov, A. A., & Rudyak, V. Y. (2016). Direct numerical simulation of the turbulent flows of power-law fluids in a circular pipe. *Thermophysics and Aeromechanics*, 23(4), 473–486.
14. Gavrilov, A. A., & Rudyak, V. Y. (2017). Direct numerical simulation of the turbulent energy balance and the shear stresses in power-law fluid flows in pipes. *Fluid Dynamics*, 52(3), 363–374.
15. Singh, J., Rudman, M., & Blackburn, H. M. (2017). The effect of yield stress on pipe flow turbulence for generalised Newtonian fluids. *Journal of Non-Newtonian Fluid Mechanics*, 249, 53–62.
16. Singh, J., Rudman, M., & Blackburn, H. M. (2017). The influence of shear-dependent rheology on turbulent pipe flow. *Journal of Fluid Mechanics*, 822, 848–879.
17. Zheng, E. Z., Rudman, M., Singh, J., & Kuang, S. B. (2019). Direct numerical simulation of turbulent non-Newtonian flow using OpenFOAM. *Applied Mathematical Modelling*, 72, 50–67.
18. Abdi, M., Noureddine, A., & Ould-Rouiss, M. (2020). Numerical simulation of turbulent forced convection of a power law fluid flow in an axially rotating pipe. *Journal of the Brazilian Society of Mechanical Sciences and Engineering*, 42(1), 1–11.
19. Hassan, M., Mebarek-Oudina, F., Faisal, A., Ghafar, A., & Ismail, A. I. (2022). Thermal energy and mass transport of shear thinning fluid under effects of low to high shear rate viscosity. *International Journal of Thermofluids*, 15, 100176.
20. Asogwa, K. K., Mebarek-Oudina, F., & Animasaun, I. L. (2022). Comparative investigation of water-based Al2O3 nanoparticles through water-based CuO nanoparticles over an exponentially accelerated radiative Riga plate surface via heat transport. *Arabian Journal for Science and Engineering*, 1–18.
21. Djebali, R., Mebarek-Oudina, F., & Rajashekhar, C. (2021). Similarity solution analysis of dynamic and thermal boundary layers: Further formulation along a vertical flat plate. *Physica Scripta*, 96(8), 085206.
22. Raza, J., Mebarek-Oudina, F., Ram, P., & Sharma, S. (2020). MHD flow of non-Newtonian molybdenum disulfide nanofluid in a converging/diverging channel with Rosseland radiation. In *Defect and Diffusion Forum* (Vol. 401, pp. 92–106). Trans Tech Publications Ltd.
23. Djebali, R., Mebarek-Oudina, F., & Rajashekhar, C. (2021). Similarity solution analysis of dynamic and thermal boundary layers: Further formulation along a vertical flat plate. *Physica Scripta*, 96(8), 085206.
24. Mebarek-Oudina, F. (2017). Numerical modeling of the hydrodynamic stability in vertical annulus with heat source of different lengths. *Engineering Science and Technology, an International Journal*, 20(4), 1324–1333.
25. Redjem-Saad, L., Ould-Rouiss, M., & Lauriat, G. (2007). Direct numerical simulation of turbulent heat transfer in pipe flows: Effect of Prandtl number. *International Journal of Heat and Fluid Flow*, 28(5), 847–861.